Available online at www.sciencedirect.com

ScienceDirect

www.elsevier.com/locate/jmbbm

Research Paper

Fretting-corrosion behavior in hip implant modular junctions: The influence of friction energy and pH variation



Dmitry Royhman^a, Megha Patel^b, Maria J. Runa^c, Markus A. Wimmer^a,
Joshua J. Jacobs^a, Nadim J. Hallab^a, Mathew T. Mathew^{a,*}

^aDepartment of Orthopedic Surgery, Rush University Medical Center, Chicago, IL, United States of America

^bDepartment of Biotechnology, University of Illinois at Chicago Medical College, Rockford, IL, United States of America

^cCenter MicroElectroMechanical Systems (CMEMS), University of Minho, Guimaraes, Portugal

ARTICLE INFO

Article history:

Received 26 September 2015

Received in revised form

24 February 2016

Accepted 18 May 2016

Available online 3 June 2016

Keywords:

CoCrMo

Ti6Al4V

Fretting

Corrosion

Modular

Implant failure

ABSTRACT

Background: Recently, there has been increasing concern in the orthopedic community over the use of hip implant modular devices due to an increasing number of reports of early failure, failure that has been attributed to fretting-corrosion at modular interfaces. Much is still unknown about the electrochemical and mechanical degradation mechanisms associated with the use of such devices.

Purpose: Accordingly, the purpose of our study was to develop a methodology for testing the fretting-corrosion behavior of modular junctions.

Methods: A fretting-corrosion apparatus was used to simulate the fretting-corrosion conditions of a CoCrMo hip implant head on a Ti6Al4V hip implant stem. The device features two perpendicularly-loaded CoCrMo pins that articulated against a Ti6Al4V rod. A sinusoidal fretting motion was applied to the rod at various displacement amplitudes (25, 50, 100, 150 and 200 μm) at a constant load of 200 N. Bovine calf serum at two different pH levels (3.0 and 7.6) was used to simulate the fluid environment around the joint. Experiments were conducted in two modes of electrochemical control – free-potential and potentiostatic. Electrochemical impedance spectroscopy tests were done before and after the fretting motion to assess changes in corrosion kinetics.

Results: In free potential mode, differences were seen in change in potential as a function of displacement amplitude. In general, V_{Drop} (the drop in potential at the onset of fretting), V_{Fretting} (the average potential during fretting), $\Delta V_{\text{Fretting}}$ (the change in potential from the onset of fretting to its termination) and V_{Recovery} (the change in potential from the termination of fretting until stabilization) appeared linear at both pH levels, but showed drastic deviation from linearity at 100 μm displacement amplitude. Subsequent EDS analysis revealed a large number of Ti deposits on the CoCrMo pin surfaces. Potentiostatic tests at both pH levels generally showed increasing current with increasing displacement amplitude. Electrochemical impedance spectroscopy measurements from free potential and potentiostatic tests indicated increased levels of resistance of the system after

*Correspondence to: 1611 W. Harrison Ave., Suite 204-H, Chicago, IL 60612, United States. Tel.: +1 312 942 5000.

E-mail address: Mathew_T_Mathew@rush.edu (M.T. Mathew).

induction of the fretting motion. In free potential tests, the largest increase in impedance was found for the 100 μm group.

Conclusions: We conclude that the 100 μm group exhibits deviations from linearity for several parameters, and this was most likely due to adhesive wear between Ti6Al4V and CoCrMo surfaces. Overall, the degradation of the system was dominated by wear at all pH levels, and displacement amplitudes.

© 2016 Published by Elsevier Ltd.

1. Introduction

Metallic biomaterials such as Ti alloys and CoCrMo alloys are widely used in total hip arthroplasty (THA) due to their relatively high biocompatibility, strong resistance to degradation when in contact with biological milieu and the absence of hypersensitivity responses in surrounding tissue (Huber et al., 2009; Hallab et al., 2001). These properties have been primarily attributed to the presence of a passive oxide film that spontaneously forms on the surface of these medical alloys (Hodgson et al., 2004; Lavos-Valereto et al., 2004). This passive film is typically a few nanometers thick and provides protection against corrosion, i.e., metal dissolution into the surrounding electrolytic environment. All metals in contact with biological systems undergo corrosion albeit, some at a much slower rate than others (Billi et al., 2012; Brown and Merritt, 1981). When the passive layer is removed, for example by a chemical or mechanical process, the result is increased dissolution of metal ions (Celis et al., 2006). Under mechanical stimulation, the oxide film on the surface can become abraded, exposing the bulk underlying alloy to the electrolytic environment, which leads to reactions that increase the corrosion rate (Barril et al., 2002; Swaminathan and Gilbert, 2012). These metal ions can activate the immune system by aggregating with endogenous proteins, which could cause an immune response and promote dermatitis, urticaria, and vasculitis (Hallab et al., 2009).

In addition to providing protection against corrosion, the surface oxide layer has properties that are different from those of the bulk alloy, and therefore may influence the mechanical behavior of the implant (Goldberg and Gilbert, 2004). This oxide film and its properties are influenced by the electrical potential of the metal (Swaminathan and Gilbert, 2012; Barril et al., 2004; Brown et al., 1988). Therefore, the passive film and its potential-dependent properties have an important role in the electrochemical and the mechanical behavior of the alloy surface (Swaminathan and Gilbert, 2012; Barril et al., 2004; Brown et al., 1988).

Modern hip prostheses feature a modular implant design with a tapered junction between the head & femoral neck, which gives the surgeon flexibility in implant assembly and reduces inventory (Cook et al., 1994). Despite their apparent benefits, however, there have been an increasing number of reports of implant failures due to the modular design, which has alarmed orthopedic patients and clinicians (Cook et al., 1994; Chandrasekaran et al., 1999; Cook et al., 2013; Brown et al., 1995). Currently, approximately 400,000 hip replacements are performed each year, and the implants have an average life span of approximately 15 years. Hence, multiple

revision surgeries may be required during the lifetime of a patient, particularly a younger patient (Kurtz et al., 2014). Most hip prostheses use metal-based alloys (Ti and CoCrMo) for femoral stems and heads (Rodrigues et al., 2009; Hu et al., 2014; Gilbert et al., 1993).

If two contacting surfaces (such as Ti and CoCrMo in hip prostheses) are subject to minute relative movements that result from the repetitive loading conditions of the implant, a special mode of wear, termed “fretting,” occurs. Since orthopedic implants are made of metallic components, increased corrosion also often occurs due to increased surface area and local chemical changes that favor metal ion dissolution and corrosion (Brown et al., 1995; Gilbert et al., 2009).

Additionally, any existing crevice at a modular junction provides favorable conditions for corrosion (Brown et al., 1995; Gilbert et al., 2009). Numerous reports have presented evidence of the combined action of fretting and corrosion at modular junctions of hip retrievals and the researchers attempted to gain a better understanding of the degradation process (Chandrasekaran et al., 1999; Cook et al., 2013; Brown et al., 1995; John Cooper et al., 2012; Kop and Swarts, 2009). The end result of these processes can be adverse biological reactions, which can cause implant failure in patients and several other complications (John Cooper et al., 2012; Cooper et al., 2013).

Some of the complications of metal ion release include: pain, soft tissue pseudotumour, instability and asymptomatic lesions (Cooper et al., 2013; Whitehouse et al., 2015). Several aseptic failures have been attributed to immunologically determined tissue reactions such as: necrosis, perivascular lymphocytic aggregates, vasculitis and osteolytic lesions (Hallab et al., 2001). This suggests that hypersensitivity of tissues to metals plays a role in aseptic loosening.

It's necessary to investigate these modular interfaces in order to increase our understanding of their degradation mechanisms so that early failures and adverse effects in patients can be avoided; especially with regards to the synergistic interactions between wear and corrosion, which can accelerate the degradation process (Mathew et al., 2012).

Although wear and corrosion are each well-established study areas for biomedical applications, their interaction is not yet well-understood. Therefore, our study addresses the following questions: How is material loss influenced by the fretting regime and how does it affect the corrosive potential? To what extent do fretting and corrosion accelerate each other (i.e., act synergistically)? Is the synergy influenced by the generated wear and corrosion products? Can a synergistic model help in the identification of implant failure pathways?.

pins were used for every test, 3 Ti alloy rods were continuously reused/cycled during testing. Therefore, to maintain constant surface topographies, the Ti alloy rods were resurfaced after each test. The CoCrMo alloy pins were wet-ground using a series of silicone carbide grinding papers up to #800, and then were polished with 6 μm and 1 μm diamond spray on texmet and nylon cloths, respectively, to obtain a mirror finish (Surface roughness (R_a) < 20 nm). The Ti alloy rods were resurfaced by wet-grinding with silicone carbide cloths up to #800 to maintain surface roughness (R_a < 80 nm). Before testing, all samples (Pins and rods) were cleaned by 10 minute agitation cycles in an ultrasonic bath in 70% isopropanol solution, followed by a 10 min agitation in deionized H_2O and, finally, air drying using a nitrogen gas stream.

2.2. Electrochemical testing

All electrochemical tests were conducted inside of a custom-made electrochemical cell constructed from polysulfone. A potentiostat (G300, Gamry Inc., Warminster, PA, USA) with a standard 3-electrode configuration was used for the corrosion measurements. A saturated calomel electrode (SCE) was used as the reference electrode, a graphite rod as a counter-electrode, and the metal alloy as a working electrode (exposed surface (5.4 cm^2)). Bovine calf serum (BCS) solution was used as the electrolyte/lubricant (Volume = 65 mL). The BCS solution contained the following: BCS (30 g/L protein), NaCl (18 g/L), Propylene Phenoxenol (30 mL/L), Tris buffer (54 g/L), and HCl (approximately 55 mL/L, or enough to bring the pH of the solution down to 7.6). Once the initial pH of 7.6 was reached, lactic acid was added to attain a pH of 3.0 for the acidic group. The samples were mounted into the electrochemical cell and the temperature of the test solution was maintained at 37 °C.

Free potential (No applied potential) and potentiostatic (Applied constant potential) tests were performed in order to study the complex interactions between fretting motion and the electrochemical properties of the materials. Potentiodynamic (Applied potential sweep) experiments were performed as a supplementary step in order to select a constant potential to be applied during potentiostatic experiments. Free potential tests were performed in order to evaluate the effect of mechanical stimulation (Fretting) on the electrochemical response. For these tests, changes in potential were monitored before, during, and after the applied fretting motion. Potentiodynamic tests were performed in order to determine the various electrochemical regions (anodic, cathodic, and passivation regions). For the potentiodynamic tests, a potential sweep was executed from -0.8 V to $+1.8\text{ V}$ (V vs. SCE) at a rate of 2 mV/s and the resultant change in current was monitored. Potentiostatic tests were performed in order to determine the synergistic interaction between the fretting motion and corrosion. Based on potentiodynamic results (More details explained in Results section), a -250 mV (vs. SCE) potential was selected for potentiostatic tests. The total exposed surface area of 5.4 cm^2 was used calculate the current density. In addition, electrochemical impedance spectroscopy (EIS) tests were performed before and after all free potential and potentiostatic tests in order to examine the change in passivation kinetics of the system in response to the applied fretting

motion. EIS measurements were performed by applying a $\pm 10\text{ mV}$ sinusoidal potential (vs. E_{oc}) from 100 KHz to 0.01 Hz.

2.3. Mechanical testing

As previously mentioned, a flat-on-flat contact (flat portion of cylinder on rectangular rod) was used. This configuration allows for a nominal contact area of 2 cm^2 (1 cm^2 per pin). With an applied force of 200 N per pin, a nominal contact pressure of 2 MPa was assumed at the articulating interface. The fretting motion was simulated by articulating a Ti alloy rod, perpendicularly against 2 CoCrMo pins (Fig. 1). The rod was attached to a servo hydraulic actuator (Model: 8871, Instron, Canton, MA, USA), which produced sinusoidal displacement waveforms, with amplitudes equal to ± 25 , ± 50 , ± 100 , ± 150 or $\pm 200\ \mu\text{m}$. The frequency of the imposed displacement was equal to 1 Hz. The tangential load and position of the Ti alloy rod was monitored and recorded (frequency of recording = 10 Hz at 10 s intervals). It is important to note that as with all laboratory fretting devices, the displacement between the articulating surfaces can deviate greatly from the intended value due to compliance of the clearances between the attached components, as well as to the elastic deformations of all the material which comprise the device. The displacements reported in this study are the nominal displacements. Fretting regime behavior (ie. Partial slip vs. gross slip) was assessed by evaluation of the tangential load and the displacement hysteresis loop behavior. A typical hysteresis cycle consists of two parts: an elastic slope and a friction plateau. The dissipated friction energy, which is defined as the area inside the hysteresis loop, is dependent on the normal load. To identify the fretting regime, the ratio of dissipated energy to total energy was utilized, as defined by Mohrbacher et al. Mohrbacher et al. (1993) Previous studies determined that a ratio of 0.2 corresponded to the transition criteria between partial slip and gross slip conditions (Fouvry et al., 1995). Fig. 2A demonstrates this relationship. A ratio higher than 0.2 is considered to be in the gross-slip regime. In contrast, a ratio less than 0.2 was considered to be in the partial slip regime.

2.4. Surface characterization

Three-dimensional images of the corroded and/or worn surfaces were obtained using a white-light interferometry microscope (Zygo New View 6300, Zygo Corporation, Middlefield, CT, USA). Images were taken before and after experiments to evaluate the physical changes that occurred as a result of the electrochemical reactions and the sliding. Changes in roughness (R_a) were compared for both Ti and CoCrMo alloys. Additional surface characterization was done using scanning electron microscopy (SEM) (Joel JSM-6490 LV, Oxford Instruments, Oxford, UK) to examine the effects of the fretting motion on the metal surfaces.

2.5. Weight loss estimation and wear-corrosion synergy

The synergistic relationship, as proposed by Stack and Abdulrahman (2010), was studied using the following relationship.

$$K_{wc} = K_c + K_w \quad (1)$$

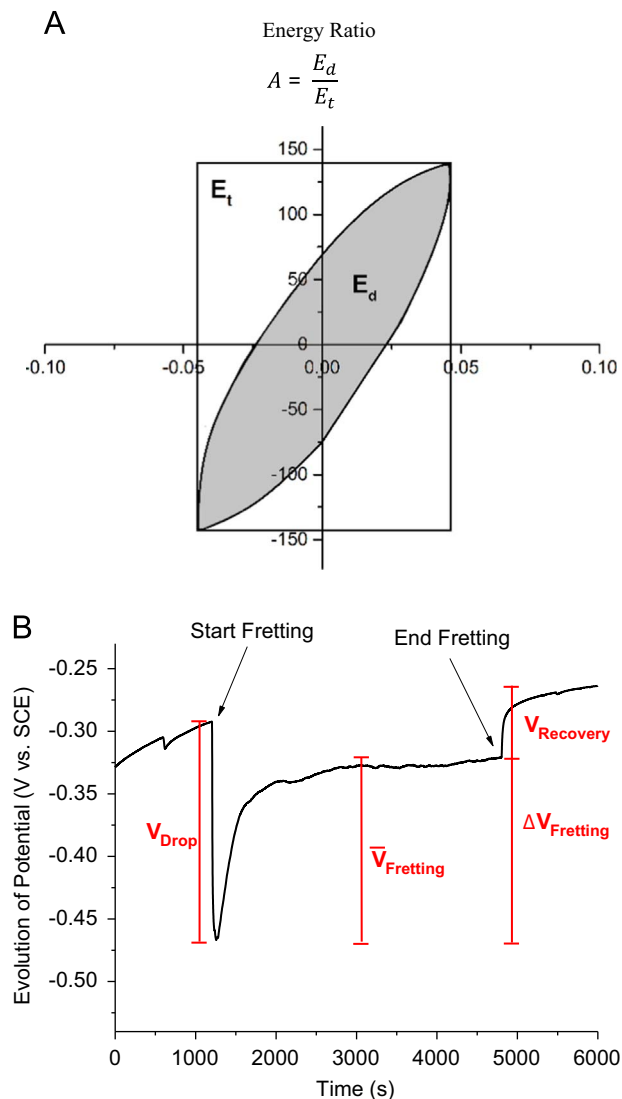


Fig. 2 – (A) Representation of the energy ratio, for which the transition criteria between partial slip and gross slip is defined at a ratio of 0.2 of the dissipated energy (E_d) to total energy (E_t). (B) A representation of the criteria used to describe the behavior of potential throughout the fretting experiment.

According to this relationship, ' K_{wc} ' (Total material loss) is the combination of ' K_c ' (Material loss due to corrosion) and ' K_w ' (Material loss due to wear). ' K_{wc} ' can be determined by analyzing the total metal content of the solution. In typical tribological contacts (ex: ball-on-flat or cylinder-on-flat), the wear scar has a conforming geometry and the weight loss estimation can be performed through profilometry. In our study, the contact was a flat-on-flat configuration. Such conditions make it difficult to make weight loss estimations with the same technique. Therefore, the material loss estimation was performed using the ICP-MS technique. A representative solution sample (1.5 mL) was collected at the end of each test for metal content analysis. The protocol for the detection and digestion methods are explained elsewhere (Dufils et al., 2015).

' K_c ' can be calculated using Faraday's equation:

$$K_c = \frac{M \times Q}{n \times f} \quad (2)$$

Where ' M ' is the atomic mass of the metal alloy, ' Q ' ($Q = \text{Current [I]} \times \text{time [s]}$) is the charge passed through the working electrode in coulombs, ' n ' is the valence of the product (we assumed $n=2$), and ' f ' is Faraday's constant ($96,500 \text{ C/mol}^{-1}$). It should be noted that this system contains two different alloys and therefore some consideration has to be made as to how to account for the current levels generated from each individual component. From previous tests performed in our lab it was shown that under similar conditions, using an electrochemically inert counterbody (Alumina), that the mass loss due to corrosion of Ti6Al4V is more than 2 orders of magnitude higher than CoCrMo (Royhman et al., 2013). Therefore, the assumption was made that the K_c contribution of the CoCrMo was negligible. In order to simplify the calculation, the Faraday equation was performed using only the properties of Ti6Al4V.

Once ' K_{wc} ' and ' K_c ' have been determined, the relationship in Eq. (1) can be rearranged to find ' K_w '.

$$K_{wc} - K_c = K_w \quad (3)$$

3. Results

3.1. Fretting corrosion under free potential mode

3.1.1. Evolution of potential behavior

The effects of mechanical stimulation on electrochemical behavior can be evaluated by monitoring the evolution of potential before, during, and after the fretting phase. To empirically describe the trends in electrochemical behavior, analysis was done on specific regions of the curves. These regions are depicted in Fig. 2B as V_{Drop} (Drop in potential at onset of fretting), V_{Fretting} (Average potential during fretting), $\Delta V_{\text{Fretting}}$ (Change in potential from onset of fretting to termination of fretting) and V_{Recovery} (Change in potential from the termination of fretting until stabilization of the metal samples). The responses in potential as a function of displacement amplitude and pH (3.0 and 7.6) are shown in Fig. 3A and B respectively. The values of V_{Drop} , V_{Fretting} , $\Delta V_{\text{Fretting}}$ and V_{Recovery} are shown in Fig. 3C-F, respectively.

In all tests, a cathodic (negative shift) drop of the potential was observed in response to the fretting motion. As shown in Fig. 3A–C, the magnitude of the drop (V_{Drop}) was determined to be a direct function of the displacement amplitude, and of the pH. In general, V_{Drop} increased with increasing displacement amplitude. A deviation from the linear trend in V_{Drop} was observed at pH 7.6 at 100 μm displacement. V_{Fretting} (Fig. 3D) was always higher in the pH 3.0 groups compared to the pH 7.6 groups. Both pH 3.0 and pH 7.6 groups exhibited an inverse correlation between V_{Fretting} and increasing displacement amplitude. $\Delta V_{\text{Fretting}}$ (Fig. 3E) increased with increasing displacement amplitude. V_{Recovery} showed a trend opposite to that of V_{Fretting} (Fig. 3F). The pH 7.6 groups were consistently higher than the pH 3.0 groups. In general, the areas of lowest average fretting potential showed the greatest tendency to recover.

3.1.2. Evolution of hysteresis behavior under free potential mode

Fig. 4A and B shows the hysteresis response of the tangential load to displacement amplitude at each cycle throughout the fretting test. The cross-sectional area of these hysteresis loops is indicative of the dissipated friction energy at the corresponding cycle. In all tests, there was an increase in the cross-sectional areas of the hysteresis loops as a function of increasing displacement amplitude.

This hysteresis behavior can be alternatively expressed as shown in Fig. 4C and D, which provide the dissipated friction energy at each cycle, shown by representative plots, for pH 3.0 and pH 7.6. The graphs confirm that there is an increase in cross-sectional area, and therefore, in the dissipated friction energy, in Joules, of each cycle, with respect to increasing displacement amplitude. The highest dissipated friction energy was seen in the pH 7.6 group at 200 μm displacement amplitude.

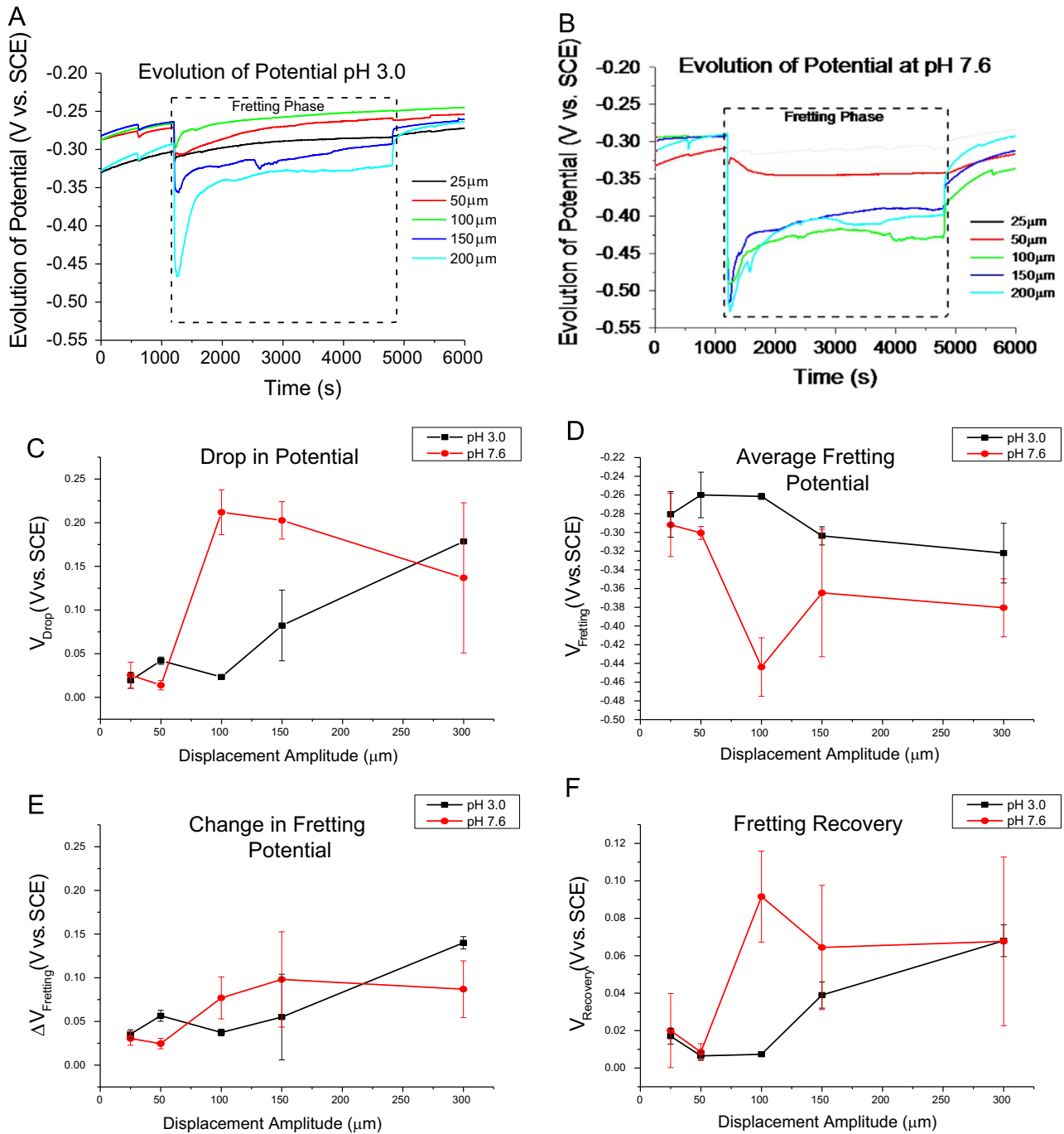


Fig. 3 – The effects of mechanical stimulation on the electrochemical behavior can be evaluated by monitoring the evolution of potential. The response in potential as a function of displacement amplitude and pH (3.0 and 7.6) is shown in (A) and (B) respectively. Specific regions of the curves such as “Drop in Potential,” “Fretting Potential,” “Change in Fretting Potential” and “Fretting Recovery,” are shown in (C)–(F), respectively.

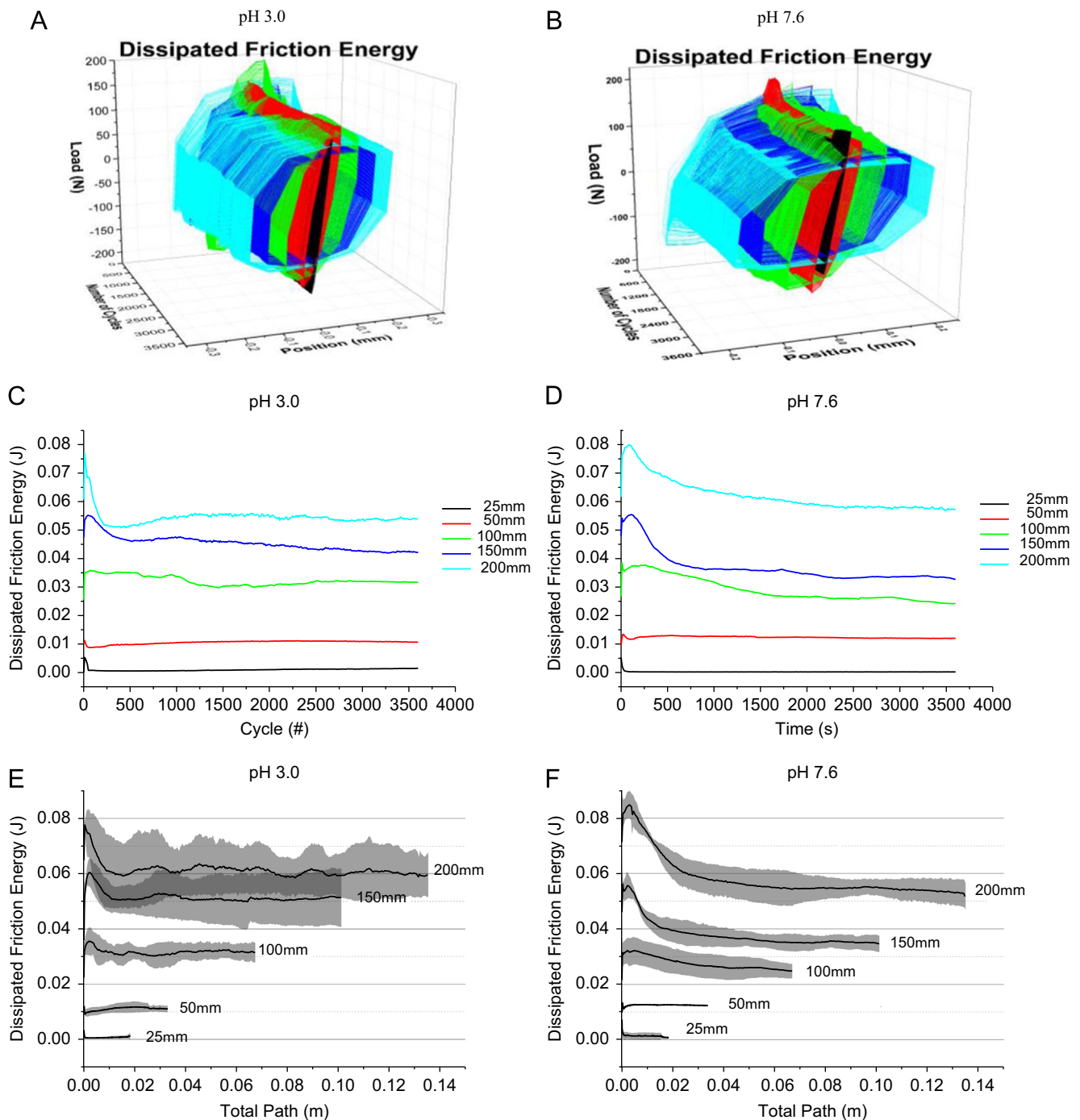


Fig. 4 – The hysteresis response, under free potential mode, of the tangential load/displacement behavior throughout the applied fretting motion at (A) pH 3.0 and (B) pH 7.6. This dissipated friction energy is shown by representative plots of dissipated friction energy in Joules at each movement cycle as a function of (C) pH 3.0 and (D) pH 7.6. Dissipated friction energy in Joules over the total distance traveled, in meters, is shown by averaged curves of all trials with standard deviations (grey) for (E) pH 3.0 and (F) pH 7.6. Darker regions indicate areas of overlap in standard deviation.

The dissipated friction energy can also be represented as in Fig. 4E and F. These panels show the amount of Joules over the total distance displaced between the metallic rod and the pins, in meters, under free potential conditions. This relationship was based on averaging the curves for all the trials in each group. The standard deviations of these trials are shown in

grey. The darker grey regions indicate overlap in standard deviations between curves. The graphs confirm the trends observed in Fig. 4A–D.

Fig. 5 depicts the relationship, between the evolution of potential and the dissipated friction energy. There was a direct relationship and robust correlation between the

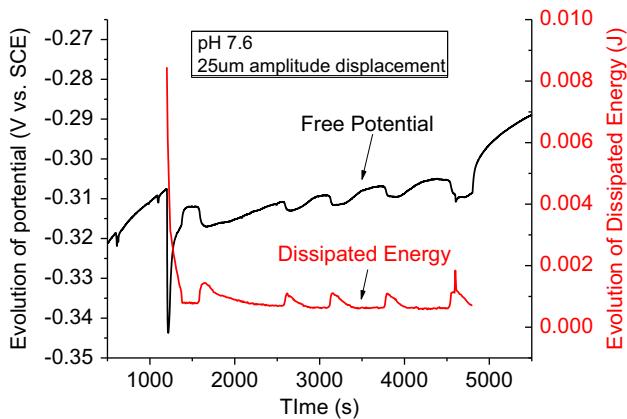


Fig. 5 – The relationship between the evolution of potential (Y1 axis) and the dissipated friction energy (Y2 axis). The two curves show a correlation in behavior. As the dissipated friction energy increases or decreases, there is a corresponding response in evolution of potential.

dissipated friction energy and the observed potential. Throughout the test, dissipated friction energy displayed deviations in observed energy.

3.1.3. Analysis of the total metal content in solution

Results for the total metal content in solution are shown in Fig. 6A and B for pH 3.0 and pH 7.6, respectively. There was a positive correlation between the displacement amplitude and the amount of metal found in solution. At pH 3.0 (Fig. 6A), there was a significantly higher concentration of Co found in the solution compared to Ti, Cr, and Mo. At pH 7.6 (Fig. 6B), there was a noticeably higher amount of Co in the 25 μm , 50 μm , and 100 μm groups compared to Ti, Cr, and Mo. At 150 and 200 μm , the levels of Co and Ti were similar. Findings of Cr and Mo did not appear to be affected by pH or displacement amplitude and were comparatively low across all groups. Fig. 6D shows the total metal content across all groups and indicates that at low displacement amplitudes, pH 3.0 shows higher material loss. However, as the displacement reaches 100 μm , the pH 7.6 groups overtake the pH 3.0 groups and exhibit higher material loss.

3.2. Fretting-corrosion under potentiostatic conditions

3.2.1. Evolution of current

Fig. 7 shows the potentiodynamic scans for the metal alloy coupled system of CoCrMo alloy pins loaded against the Ti6Al4V rod at pH 3.0 and pH 7.6. The data show that the coupled system reached an equilibrium potential of approximately -500 mV (vs. the SCE) at both pH levels and started to passivate at approximately 0 mV (vs. the SCE). These data were used to select the potential during the potentiostatic scan. To induce cathodic currents, but avoid passivation behavior, all potentiostatic tests were conducted at -250 mV (vs an SCE) for all groups. For the potentiostatic tests, the potential was held constant and the changes in current were monitored as the system response to the fretting motion. Fig. 8A and B shows the results of the potentiostatic tests at pH 3.0 and pH 7.6, respectively. At the

onset of fretting, there was an increase in evolved current. The current was dependent on the pH and displacement amplitude. Higher current was seen in correlation with increasing displacement amplitude. In all experiments, the corresponding displacement amplitudes showed higher current evolution at pH 3.0 than pH 7.6. Fig. 8C and D shows the evolution of current at pH 3.0 and pH 7.6, respectively, with the corresponding dissipated friction energy at each time point. The curves of evolved current are representative curves for each group, smoothed using 25 point adjacent averaging. The data indicate that there is a direct relationship between the amount of evolved current and the amount of dissipated friction energy released at each corresponding time point. As the dissipated friction energy increases, the amount of evolved current increases as well. Both the evolution of current curves and the dissipation of energy curves show an initial sharp rise, followed by a steady decline, and a final stabilization period. There were no significant differences between the dissipated friction energy released at pH 3.0 compared to pH 7.6; however, the evolved current was significantly higher at pH 3.0.

3.2.2. Fretting hysteresis loop

The mechanical, elastic-sliding response of the coupled system was evaluated by the hysteresis behavior of the tangential load vs. displacement, as described by Mohrbacher (Mohrbacher et al., 1993). The energy ratio can be described as the ratio of the dissipated friction energy to the area of average measured tangential force, multiplied by the maximum displacement. This relationship is shown in Fig. 2A. A ratio of 0.2 indicates a transition from partial slip (<0.2) to gross-slip (>0.2) regimes (Fouvry et al., 1995). The change in hysteresis behavior throughout the tests is shown in Fig. 4A and B for free potential mode for pH 3.0 and pH 7.6, respectively. At each corresponding cycle, the area inside the loops determined the dissipated friction energy.

Fig. 9 shows the dissipated friction energy under potentiostatic conditions in Joules at each cycle of the fretting motion. The relationship is based on averaged curves of all the trials in each corresponding group for (A) pH 3.0 and (B) pH 7.6. In general, all of the curves had similar values for the free potential and potentiostatic groups. The values were not dependent on the applied potential, but were highly dependent on the displacement amplitude.

Fig. 10A and B shows the energy ratios (Depicted in Fig. 2A) of the hysteresis behavior at each cycle. The data is shown by averaged curves of all trials for each corresponding group. At 25 μm displacement, the samples were within the partial slip regime (Energy ratio <0.2) throughout the entire imposed fretting motion. At all displacements higher than 25 μm , the system was within the gross-slip regime.

Analysis of the dissipated friction energy showed that all groups showed an initial, elevated, amount of dissipated friction energy, and after 1–2 hundred cycles, the system reached a stable state. In general, the dissipated friction energy increased with increasing displacement amplitude at both pH levels. Additionally, the pH 7.6/200 μm group showed the highest amount of dissipated friction energy.

Fig. 10A and B shows the energy ratio of each group for pH 3.0 and pH 7.6, respectively. The data show that there were no differences between pH levels. However, there were differences

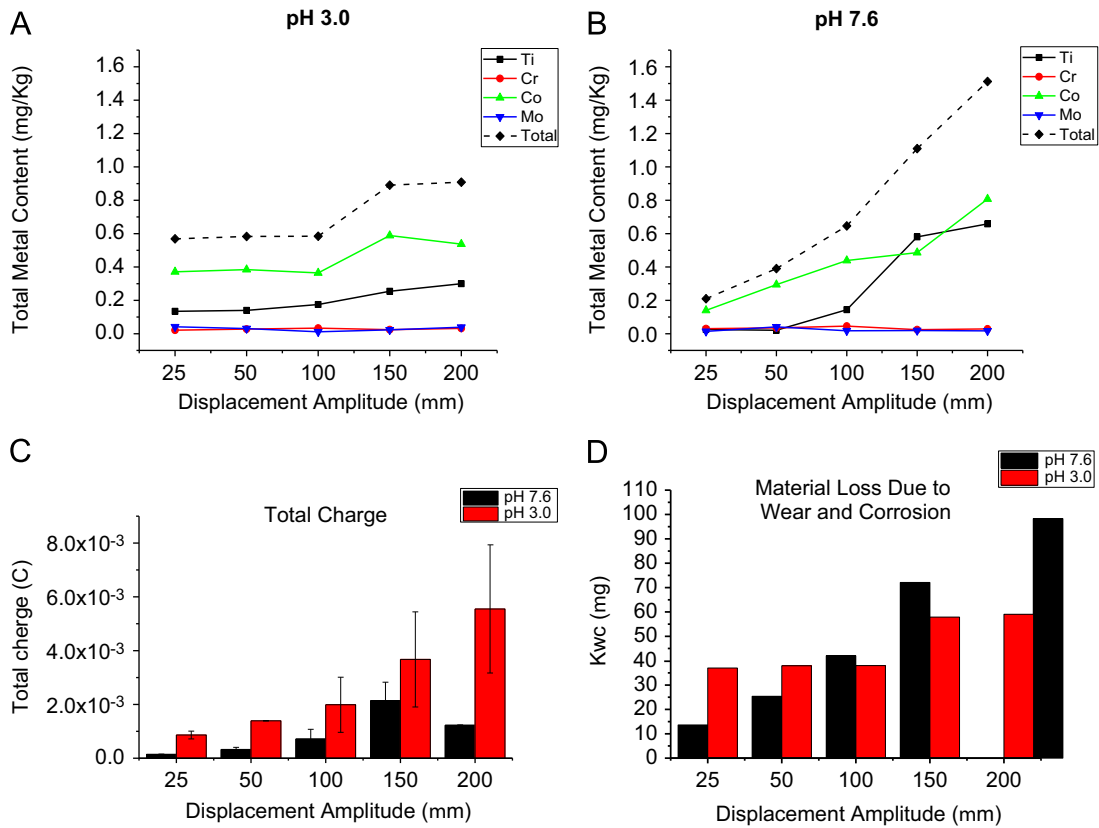


Fig. 6 – Total metal content (ions and particles) of Ti, Co, Cr, Mo and their total sum in solution at the conclusion of the potentiostatic tests at pH (A) 3.0 and (B) pH 7.6, analyzed by ICM-MS. Total charge (C) and total material loss (K_{wc}) (D) during the fretting corrosion test.

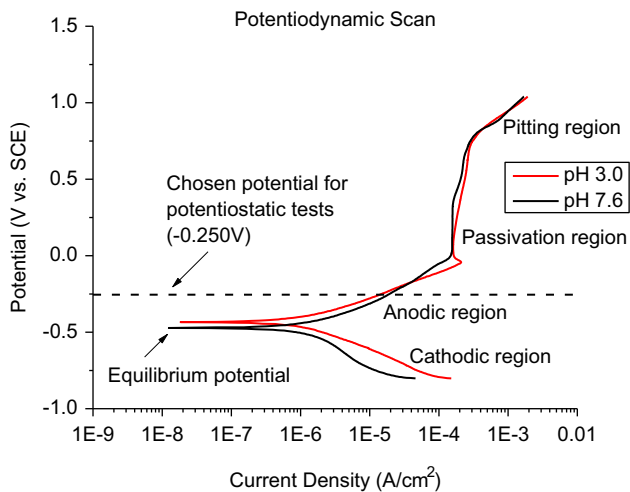


Fig. 7 – Potentiodynamic scans, at pH 3.0 and pH 7.6, for the metal alloy coupled system of CoCrMo alloy pins loaded against a Ti6Al4V rod.

observed between displacement amplitudes. In general, the energy ratio increased with increasing displacement amplitude. Of all tested conditions, only the 25 μm groups were in the partial slip regime. All other groups were in the gross slip regime.

3.2.3. EIS data analysis

The EIS technique was used both before and after the fretting corrosion tests to characterize the effect of the fretting motion on the electrochemical kinetics at the metal/electrolyte interfaces. An equivalent circuit model was used to attain a quantitative measure of the impedance of the system (opposition to the flow of alternating current), including the energy storage (capacitance) and dissipation (resistance) properties. Fig. 11A shows the composition of the electrochemical equivalent circuit used for modeling the EIS data. The representative properties of the electrolytic solution and two alloys were incorporated into the model as: R_{sol} (resistance of the solution), CPE_{Ti} (Capacitance of the Ti alloy passive film), R_{Ti} (Resistance of the Ti alloy passive film), CPE_{CoCr} (Capacitance of the CoCrMo alloy passive film), R_{CoCr} (Resistance of the CoCrMo alloy passive film). Fig. 11B and C shows a single representative EIS result, presented as Bode and Nyquist plots, respectively. The data suggested that there are two time constants present in the system. It was postulated that the secondary time constant may be due to complex interactions between the individual passive film properties of the two alloys or any associated crevices that may be present when they are engaged. In either scenario, this complex behavior was observed in all groups and repeats and the unique equivalent circuit showed a good fit across the spectrum. The total resistance of the system is presented numerically in Fig. 11D–G.

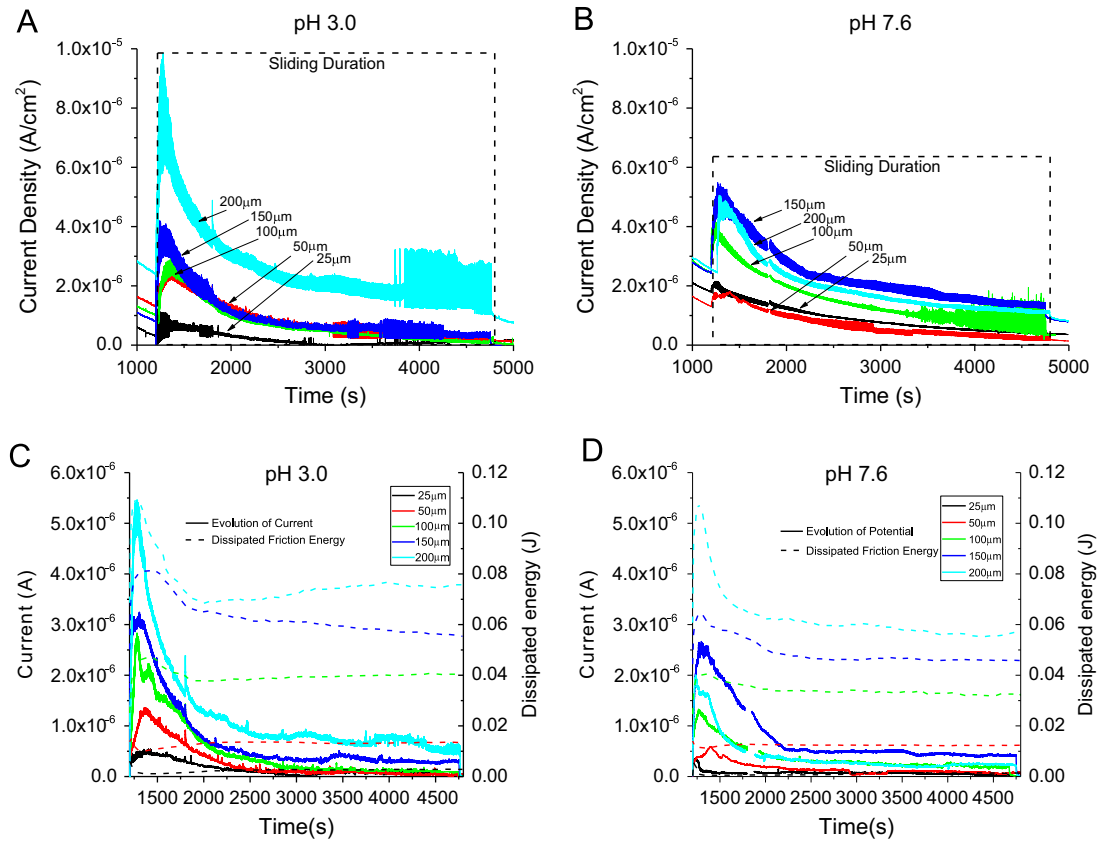


Fig. 8 – Changes in current evolution as a function of sliding distance under potentiostatic mode at (A) pH 3.0 and (B) pH 7.6. Comparison of evolution of current (Y1 axis; smoothed curves using 25 point adjacent averaging) under potentiostatic mode compared to the dissipated friction energy (Y2 axis) at the corresponding time point at (C) pH 3.0 and (D) pH 7.6.

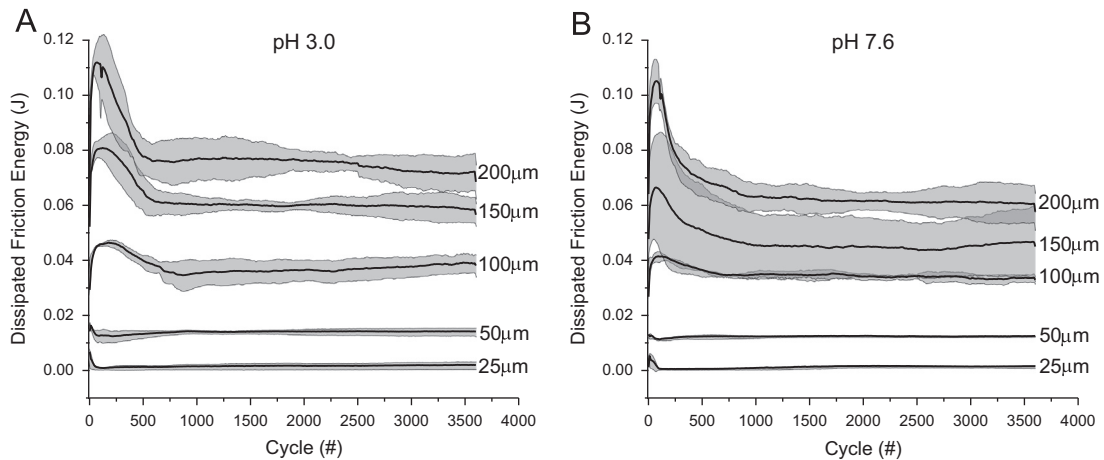


Fig. 9 – Dissipated friction energy under potentiostatic mode, in Joules, as a function of cycle number, shown by averaged curves of all trials, with standard deviations (grey), for (A) pH 3.0 and (B) pH 7.6. Darker areas indicate regions of overlap in standard deviation.

The amount of resistance is proportional to the thickness or protectiveness of the passive layer. This is physically represented as less corrosion occurring on the metal surface. The graphs indicate several distinct trends in resistance behavior. Under free potential conditions, the resistance of the system was generally increased after the fretting motion.

There was no correlation between the displacement amplitude and the amount of increase in resistance. However, at both pH levels at 100 μm displacement amplitude, there was a much higher increase in resistance compared to all other displacement amplitude groups. No significant differences in resistance were observed as a function of pH.

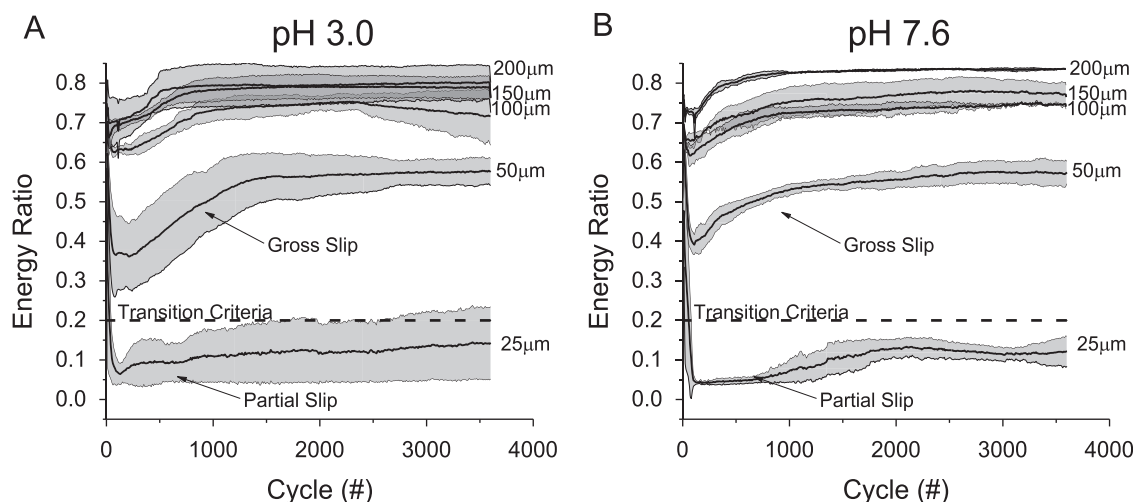


Fig. 10 – Energy ratios of displacement amplitudes under potentiostatic mode shown as function of cycle number, is shown by averaged curves of all trials, with standard deviations (grey), for (A) pH 3.0 and (B) pH 7.6. Darker areas indicate regions of overlap in standard deviation.

The resistance values under potentiostatic mode exhibited drastically different behavior compared to free potential conditions. First, at pH 3.0, there were no differences between resistance measurements before and after the fretting corrosion tests. However, at pH 7.6, there was an increase in resistance after the fretting corrosion tests. In addition, there was a positive correlation between (i) the amount of resistance, measured after the fretting corrosion test, and (ii) the displacement amplitude. Finally, in contrast to free potential conditions, under potentiostatic conditions there was a strong correlation between the amount of resistance and pH level. All resistance values were significantly higher at pH 7.6 compared to pH 3.0.

3.3. Surface analysis

Fig. 12 shows the changes in surface roughness at the CoCrMo pin from free potential tests as a function of displacement. In general, pH 3.0 groups showed higher surface roughness in all groups compared to pH 7.6 groups. In addition, the surface roughness increased with increased displacement amplitude. A deviation from the linear trend is seen at 100 μm at both pH levels,

Fig. 13A shows scanning electron micrographs of the fretting wear scars. At 25 μm the pH 3.0 samples showed severe cracking. The same group at pH 7.6 showed typical fretting scar behavior and also displayed periodic, synchronous blobs of carbonaceous material on the surface. At 50 μm , samples at both pH's showed distinct wear tracks, with some cracking inside the wear tracks, as well as some isolated pits. At 100, 150, and 200 μm displacement, the wear scars were indistinguishable from a sliding-wear behavior. Fig. 13B shows the atomic percent of Ti found in the wear scar regions of the CoCrMo pins, determined by EDS analysis. The results indicate that there was a marked increase in Ti percent in the 100 μm group for both pH levels compared to all other groups. The pH 7.6 groups showed a higher percent of Ti on the CoCrMo pins compared to pH 3.0 at all displacements except 200 μm .

4. Discussion

4.1. Variations in evolution of potential and fretting loop as a function of displacement amplitude and pH levels

The free potential tests (no potential is applied to the metal alloys) were used to study the effects of mechanical stimulation on the electrochemical behavior of Ti and CoCrMo alloys. Fig. 3 shows the results of the free-potential tests.

A drop in potential has been well-reported in the literature under both sliding and fretting conditions (mechanical stimuli) in both Ti and CoCrMo alloys (Geringer et al., 2005; Royhman et al., 2013; Butt et al., 2015; Mischler, 2008; Mathew et al., 2015). This cathodic drop is associated with removal of the passive film, due to the mechanical disruption of the film (Barril et al., 2002; Landolt et al., 2001; Cao et al., 2015). Hence, it's expected that as the displacement amplitude increases, more passive film will be removed, and a higher potential drop will be observed. The findings agree with this expectation.

Another significant finding is the variance in potential drop between pH 7.6 and pH 3.0. Fig. 3C shows that pH 3.0 has a linear, direct, relationship between potential drop and displacement variation. At pH 7.6, the relationship is not direct and is significantly different from pH 3.0 at 50, 100 and 150 μm groups. Furthermore the potential drop is significantly higher at 100 and 150 μm in pH 7.6 compared to pH 3.0. This trend may be explained by the difference in passivation kinetics that occur between acidic and neutral environments as well as the transfer of material from the Ti rod onto the CoCrMo pins, which can further complicate the passivation mechanism. Several studies have shown the delayed or inhibited formation of passive film on the surface of passive metals in acidic conditions (Royhman et al., 2014).

In addition to the variable rate of passivation, the testing conditions also displayed a variation in passive layer physical removal. This was due to that fact that, in all tests, the frequency of motion remained at 1 Hz. However, the displacement

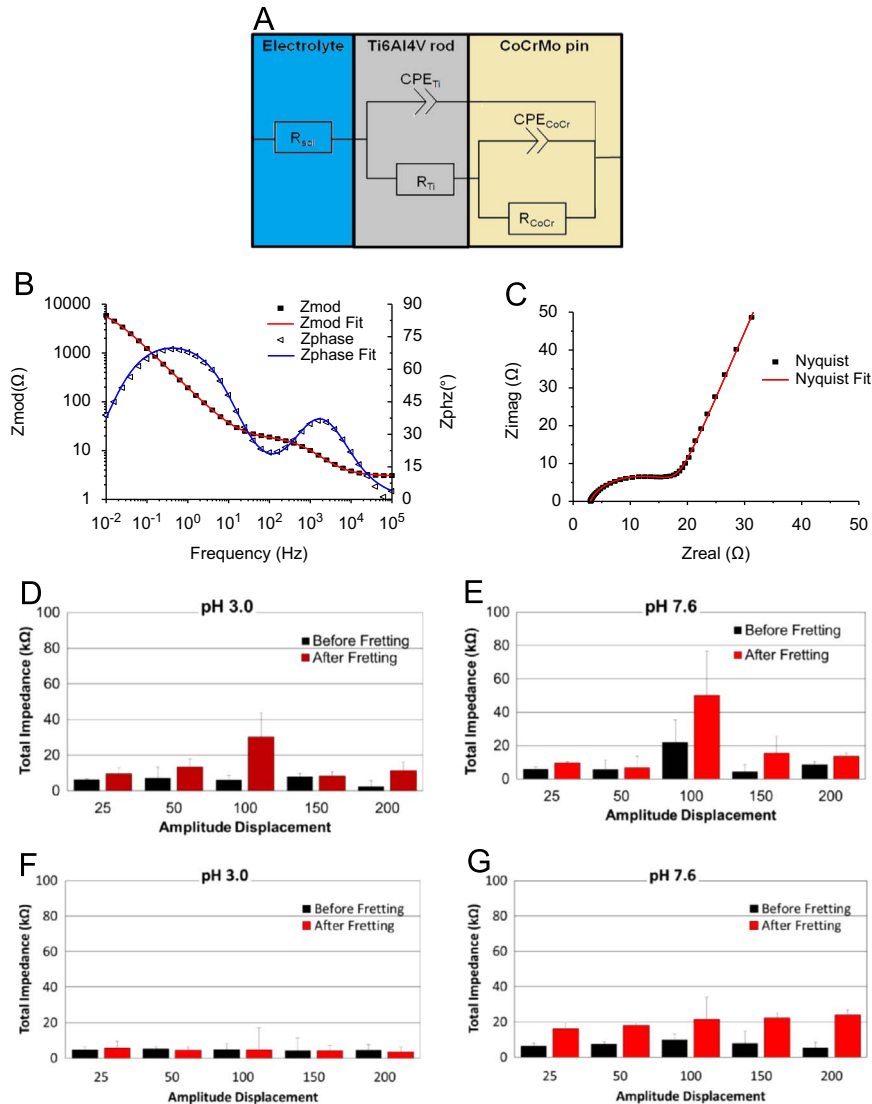


Fig. 11 – (A) Electrochemical equivalent circuit used for modeling the EIS data. The representative properties of the two alloys were incorporated into the model with individual components for: R_{sol} (resistance of the solution), CPE_{Ti} (Capacitance of the Ti alloy passive film), R_{Ti} (Resistance of the Ti alloy passive film), CPE_{CoCr} (Capacitance of the CoCrMo alloy passive film), R_{CoCr} (Resistance of the CoCrMo alloy passive film). A single representative EIS result is presented as Bode and Nyquist plots are shown in (B) and (C), respectively. All EIS results, under free potential mode, are shown as numerical values, before and after fretting, at (D) pH 3.0 and (E) 7.6. All EIS results, under potentiostatic mode, are shown as numerical values, before and after fretting, at (F) pH 3.0 and (G) 7.6.

amplitude at each cycle was different for each group (25, 50, 100, 150, and 200 μm). Therefore, the velocity of the relative articulating motion was different for each displacement amplitude. Therefore, the transient response in potential drop at pH 7.6 may be due to the complex interaction between the rate of physical removal of the passive layer, the rate of formation of the passive film, the differences in the dynamic friction of the system, and possible changes in the lubrication regime. At pH 3.0, where the chemical environment may inhibit passive layer formation, the normal, linear, trend is observed. Similar to the potential drop, other changes in potential behavior such as average fretting potential, change in fretting potential, and fretting recovery are also affected by the chemistry of the environment. Fretting potential (Fig. 3D) decreases as a function of displacement. This indicates a decrease in the corrosion

resistance of the metal couple, at higher displacements. Fig. 3E indicates that the increase in potential drop also shows a corresponding change in potential during the fretting phase, which is controlled by the passive layer. Therefore, with increasing potential drop, there is also an increasing thermodynamic driving force to return to equilibrium. This is physically manifested as the chemical reformation of the passive layer.

Fig. 4A-F shows that the dissipated friction energy increased with increasing displacement amplitude at both pH levels. No differences in friction energy were observed between pH 3.0 and 7.6. This indicates that the changes in the passivation behavior on the surface did not affect the dissipated energy of the system. SEM observations and Energy ratio plots confirmed that only the 25 μm group was within the partial-slip regime, which was demonstrated by stick and slip deformation wear patterns. As

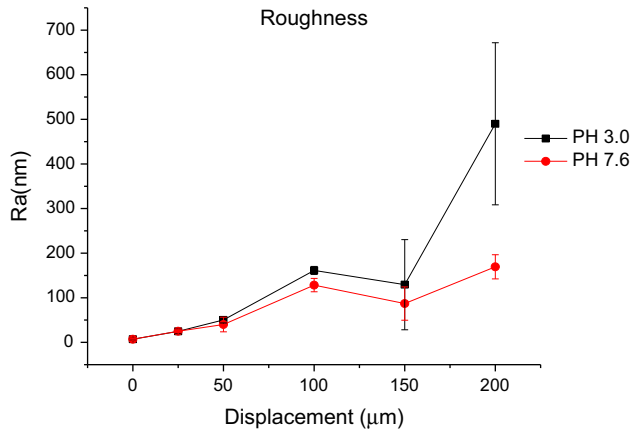


Fig. 12 – Changes in surface roughness of the CoCrMo pins as a function of displacement amplitude under free potential mode.

the displacement increased to 50 μm, the regime changed to gross-slip, and continued for increasing displacements.

4.2. Variations in evolution of current and hysteresis behavior as a function of pH levels

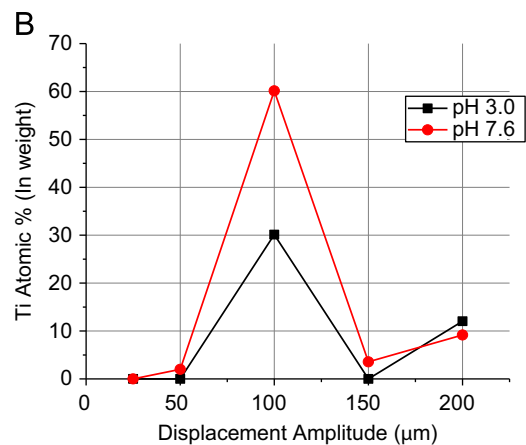
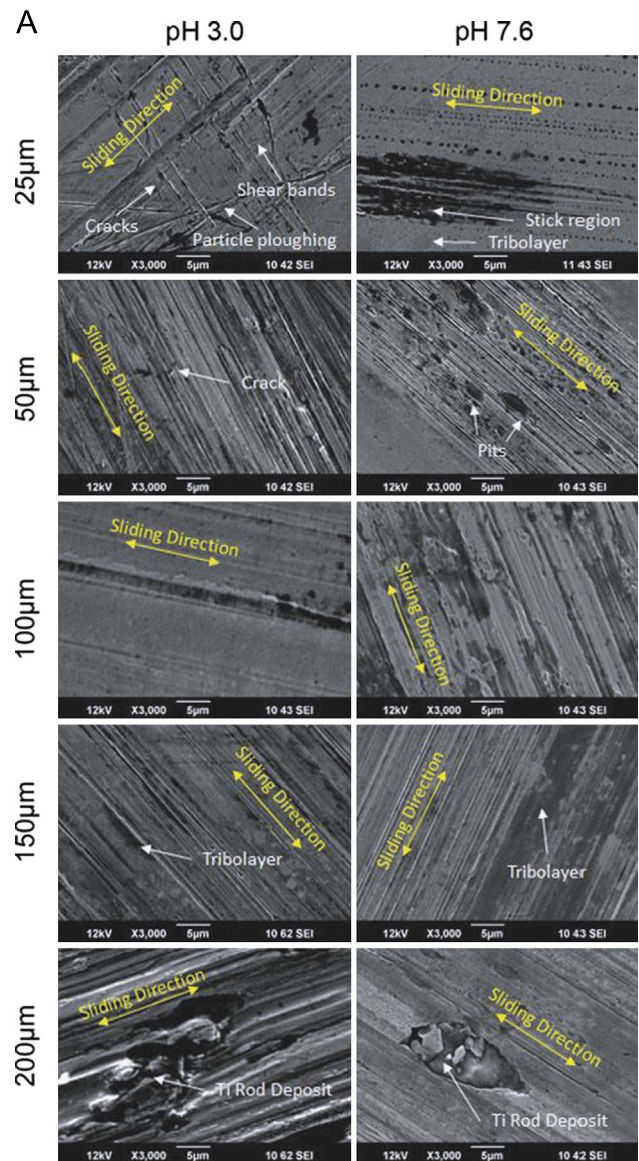
In a potentiostatic test, a pre-selected potential is applied (based on the potentiodynamic curves) and the current flowing through the working electrode (pins-CoCrMo and vertical rod-Ti alloy) is measured. Thus, this technique is very useful to understand the effect of applied potential and wear-corrosion synergism.

Fig. 8A and B shows the evolution of current as a function of displacement at pH 7.6 and 3.0 respectively. The curves show increased fluctuations in current throughout the entire test. In addition, there was an initial, sudden peak in current when the fretting motion began, which progressively diminished throughout the duration of the test. In addition, the sudden increment is closely related to the sliding amplitude. Increasing the sliding amplitude was positively correlated with peak current values.

The overall current evolution is lower at pH 7.6 than at pH 3.0. According to Faraday's law, the corrosion loss and metal ion release are directly proportional to the evolution of the current (Swaminathan and Gilbert, 2012). This shows that generally, during fretting, the corrosion loss is increased, and reaches a maximum during the initial, run-in portion of the mechanical motion.

Fig. 13 – (A) SEM images of the wear scar regions of the CoCrMo pins after fretting corrosion test for each pH and displacement amplitude group. At 25 μm groups, several fretting features can be seen. At high amplitude displacements (150–200 μm), sliding wear predominates, and tribolayer formation occurs. Particle deposits from the counterbody (Ti-alloy rod) were observed in the 200 μm groups. (B) the corresponding EDS findings of the atomic percent (in weight) of Ti deposited onto the CoCrMo pins.

Previous studies showed similar trends in the current under potentiostatic conditions (Lim et al., 1987; Geringer et al., 2009). However, the selection of a potential plays an integral role in current evolution. This is evident from the



potentiodynamic curves, where the electrochemical domains of the metal are clearly identified. From these results, the cathodic, anodic and passive regions of the material can be identified as can other domains such as pitting domains. Passivation kinetics play an important role in the tribocorrosion behavior of the materials. Under mechanical stimuli, the oxide layer is abraded, and passive film re-forms in order to bring the system back into a more thermodynamically stable state. This process is known as re-passivation. The fluctuations in the current in Fig. 8 highlight the variation in corrosion kinetics as the passive layer undergoes transitions between abrasion, reformation and stabilization. During each fretting cycle motion, various electrochemical mechanisms occur periodically and influence the degradation of the materials. In this study, greater damage was observed at pH3.0, as indicated by the roughness measurements (Fig. 12) and increased levels of evolved current and overall charge (Fig. 6C). These findings indicate the role of corrosion kinetics on the degradation process. These findings can be explained by the Pourbaix diagram for Ti and Cr (the main passivating elements of the system). At pH3, the Pourbaix behavior corresponded to an active dissolution region, compared to pH 7.6, which corresponded to a passive region (Pourbaix, 2013).

In addition, fretting amplitude is directly linked with increased dissipation of energy and increased abrasion of the surface oxide layer. The amount of damage is highly dependent on mechanical parameters such as, load, frequency, environmental factors and sliding velocity. This suggests that the electrochemical condition can influence the severity of the mechanical damage and induce changes in the fretting-corrosion mechanisms (Fig. 14).

4.3. Possible clinical implications concerning the hip modular junctions

This study featured a parametric evaluation of the fretting-corrosion behavior of hip implant modular junctions. Micro-motion is expected after surgery in poorly fixed devices, due to normal kinematic motion of the hip such as walking, stair climbing, sitting, etc. In general, once there is any motion between the fixed surfaces of the modular interface, the degree of relative motion tends to propagate over time as the material wears down and the system takes on a more dynamic nature. Initially, there could be a minute (fretting) motion at the interface, which can escalate to a full sliding motion, enhanced implant degradation, loss of stability of the implant, and overall implant failure. Hence, this study deals with a wide range of displacement amplitudes (25–200 μm) to evaluate the changes that can occur at these junctions over time. To simulate crevice conditions and acidic conditions of an infected joint, a low pH of 3.0 was tested and compared to conditions at neutral pH levels (pH=7.6). This study shows the significant variation in fretting-corrosion responses as a function of displacement and pH. The effect of the fretting-corrosion synergism in the overall degradation mechanism was evident from the study. During the experiments, we observed non-linear behavior of electrochemical parameters, which could be directly correlated with mechanisms of wear (fatigue, abrasion, adhesion, and tribochemical reactions). The results raise some concerns over the overall stability and performance of the modular junction, as various mechanisms and modes of wear and corrosion were observed. These results can be correlated with the complex clinical findings of retrieved samples, which also show a multifactorial cause and effect relationship.

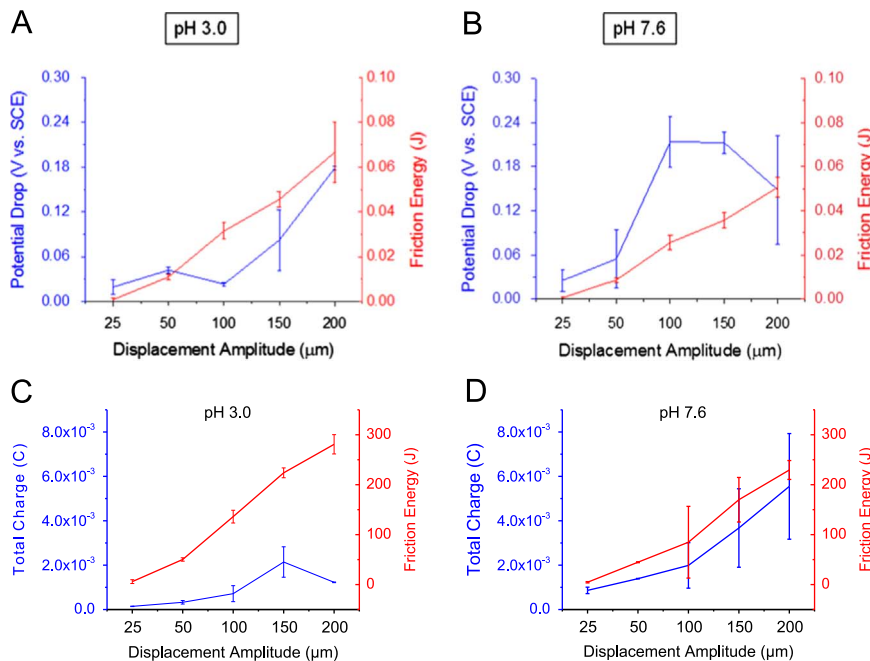


Fig. 14 – Drop in potential during the fretting-corrosion test for the Ti6Al4V-CoCrMo alloy couple at various displacement amplitudes for free potential tests at (A) pH 3.0 and (B) pH 7.6 and potentiostatic tests at (C) pH 3.0 and (D) pH 7.6. The corresponding friction energies for each group at each condition are plotted on the secondary Y (right) axes.

4.4. Transitions in the dominant failure mechanism

One of the main contributions from this study is identification of a way to obtain in-situ information on the combined effects of corrosion and friction energy. Tribocorrosion studies assist in obtaining a deeper understanding of the synergistic interaction of wear and corrosion, which could lead to increased damage of the materials of hip modular junctions. In this study, the wear-corrosion synergism was evaluated. The summary of the results is shown in Table 2. In all cases, the data suggested that the system was wear-dominated. There was some influence of pH on the corrosion behavior of the system; however, the total mass loss due to corrosion was negligible compared to the mass loss due to wear. Other studies have had similar findings of a wear dominated mechanism (Barril et al., 2004; Oladokun et al., 2015).

Fig. 15 summarizes the general findings of this study. The CoCrMo pins are loaded against a Ti6Al4V rod, which undergoes various displacement amplitudes in the vertical direction. The apparent contact consists of the entire surface area of the CoCrMo pins; however, the real contact is just at the asperities between the Ti6Al4V rod and the CoCrMo pins. During the applied motion, the nature of the wear mechanism is dependent on the displacement amplitude. Under low displacement amplitudes (25 μm), the contact undergoes elastic deformation, with the Ti6Al4V rod deforming more than the CoCrMo pins due to the lower elastic modulus. This constitutes the partial slip regime and a fatigue wear mechanism ensues. As the displacement increases to moderate levels, the gross slip regime begins to dominate the contact. Under these conditions, our setup has demonstrated large amounts of material transfer of the lower elastic modulus material onto the higher elastic modulus material. As the displacement amplitude further increases, there is a sufficient amount of dissipated energy to cause ejection of the adhered material from the interface. It has been demonstrated that an increase of the applied sliding amplitude will promote an increase of the debris ejection rate in adhesive wear tribocouples (Fouvry et al., 2007).

Gilbert et al., has reported on the adhesive wear mechanisms of Ti transferred from the femoral stems onto the CoCrMo heads in implant retrievals. In fact, the EDS results show a $\sim 54\%$ weight transfer of Ti onto the CoCrMo interface (Gilbert et al., 1993). This is comparable to our own EDS findings (Fig. 13), which show $\sim 60\%$ at pH 7.6 and $\sim 30\%$ at pH 3.0. This observation of adhesive wear associated with a specific dissipated energy (in Ti6Al4V/CoCrMo couples) may have broad implications for our understanding of the failure mechanisms of mixed metal hip implants in the clinical setting. In addition, the corresponding electrochemical findings of the deviations in electrochemical parameters in these adhesive wear groups may further help elucidate the complex pathways of failure. As was shown earlier, the group that showed high amounts of adhesive wear (100 μm), also showed deviations in potential behavior, dissipated friction energy, impedance, and roughness. Such deviations are characteristic of the complex mechanical and electrochemical changes occurring at the surface.

4.5. Limitations

There are several limitations to this study. First, the metal content analysis was done by sampling the solution after the fretting-corrosion tests. The results have shown that some adhesive wear occurred, whereby some of the metal was transferred from one articulating surface to another (Ti6Al4V rod to CoCrMo pin). Therefore, this transferred metal could not be quantified by measuring the metal content in solution, which could lead to an underestimation of the amount of material loss. Second, the flat-on-flat contact used in this study did not allow for quantification of a defined contact pressure due to the presence of the asperities present at the surface, which likely inhibited some areas of the pins from complete engagement. A nominal contact pressure was assumed for all tests. Furthermore, it is possible that the real contact area increased as the asperities were degraded throughout the test, giving a lower contact pressure at the end of the test. In addition, the Farady's equation (Eq. 2) was used to calculate the mass loss due to corrosion (K_c). Several Assumptions were made in order to

Table 2. – Summary of experimental results. Fretting regime, evaluated by energy ratio and SEM topography, determined that partial slip regime occurred at 25 μm groups at both pH levels. All other groups displayed gross slip behavior. K_c/K_w ratios indicated that wear was dominant factor of degradation with relatively little contribution was observed from corrosion (i.e. no synergism was observed under tested conditions).

	pH	25 μm	50 μm	100 μm	150 μm	200 μm
Fretting regime	3.0	Partial slip	Gross slip	Gross slip	Gross slip	Gross slip
	7.6	Partial slip	Gross slip	Gross slip	Gross slip	Gross slip
K_c (μg)	3.0	0.0 (0.0)	0.1 (0.0)	0.2 (0.1)	0.6 (0.1)	0.3 (0.0)
	7.6	0.2 (0.0)	0.4 (0.0)	0.5 (0.3)	1.0 (0.4)	1.5 (0.6)
K_{wc} (μg)	3.0	37.0	37.9	38.0	57.9	59.0
	7.6	13.6	25.4	42.0	72.1	98.3
K_w (μg)	3.0	37.0	37.8	37.8	57.3	58.7
	7.6	13.4	25.0	41.5	71.1	96.8
K_c/K_w	3.0	0.0	0.0	0.0	0.0	0.0
	7.6	0.0	0.0	0.0	0.0	0.0
Dominant mechanism	3.0	Wear	Wear	Wear	Wear	Wear
	7.6	Wear	Wear	Wear	Wear	Wear

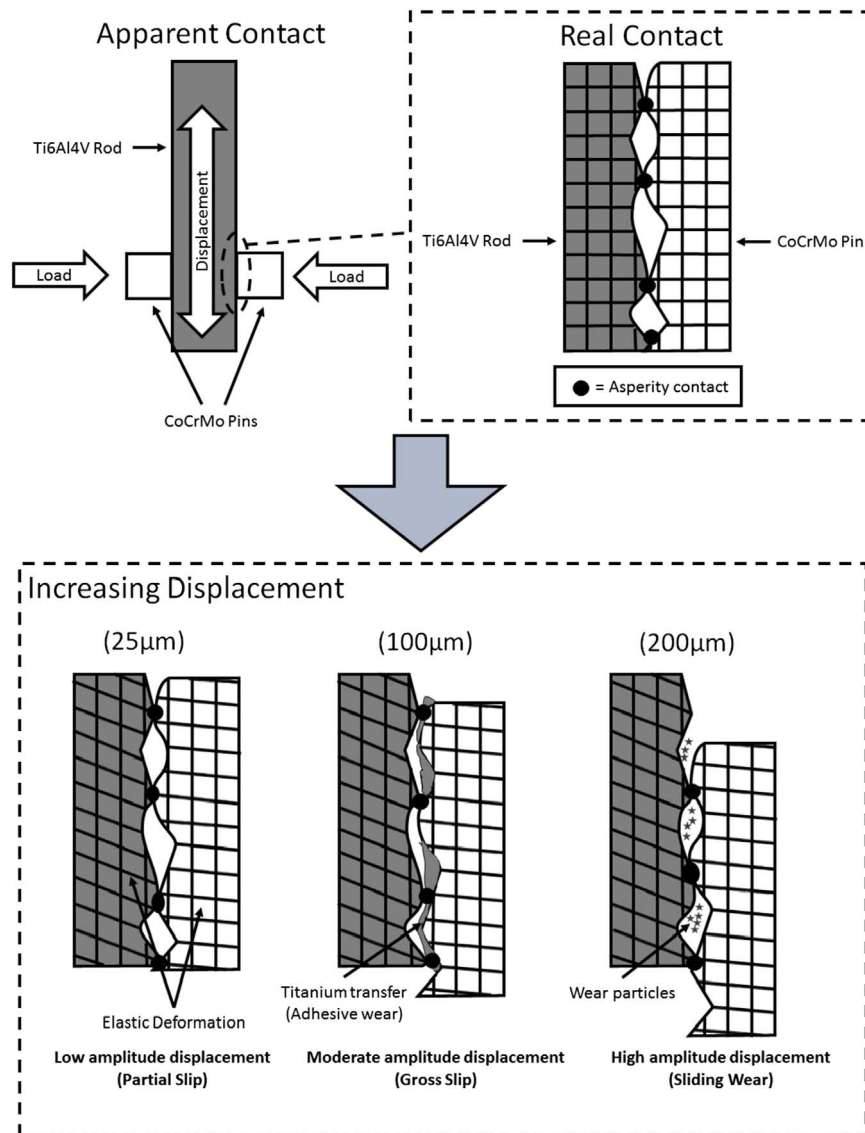


Fig. 15 – Degradation mechanisms in the experimental setup as a function of displacement amplitude.

simplify the calculation. In practice, this equation represents an idealized system with pure materials. Therefore, there may have been some differences between the estimated and real amount of material loss due to corrosion. Finally, a standard normal load of 200 N was used in these experiments at all applied displacements. Different applied loads may yield different results as they can change the real contact area of the system.

5. Conclusions

The main findings from the study can be summarized as follows;

- Electrochemical resistance was increased after fretting-corrosion stimulation.
- In general, the potential drop and evolved current were increased as a function of displacement amplitude, which could be attributed to the increased abrasion of the passive film.

- Resistance to polarization was increased after the fretting corrosion stimulation, which could be attributed to the tribochemical processes occurring on the surface, such as a deposition of a tribofilm.
- The 100 μm group demonstrated deviations from the linear trend in evolution of potential behavior, friction energy, impedance, and roughness, and this was most likely due to an adhesive wear mechanism between Ti6Al4V and CoCrMo.
- The degradation of the system was determined to be wear dominated at all pH levels, and displacement amplitudes.

Acknowledgments

The authors would like to acknowledge financial support from NIH-R03 AR064005 (to MTM). CoCrMo alloy samples were provided by Carpenter Inc.

REFERENCES

- Barril, S., Debaud, N., Mischler, S., Landolt, D., 2002. A tribo-electrochemical apparatus for in vitro investigation of fretting-corrosion of metallic implant materials. *Wear* 252 (9), 744–754.
- Barril, S., Mischler, S., Landolt, D., 2004. Influence of fretting regimes on the tribocorrosion behaviour of Ti6Al4V in 0.9 wt% sodium chloride solution. *Wear* 256 (9–10), 963–972.
- Billi, F., Onofre, E., Ebramzadeh, E., Palacios, T., Escudero, M.L., Garcia-Alonso, M.C., 2012. Characterization of modified Ti6Al4V alloy after fretting-corrosion tests using near-field microscopy. *Surf. Coatings Technol.* [Internet] [cited 28.03.13]; Available from (<http://www.sciencedirect.com/science/article/pii/S0257897212009127>).
- Brown, S.A., Flemming, C.A.C., Kawalec, J.S., Placko, H.E., Vas-saux, C., Merritt, K., et al., 1995. Fretting corrosion accelerates crevice corrosion of modular hip tapers. *J. Appl. Biomater.* 6 (1), 19–26.
- Brown, S.A., Hughes, P.J., Merritt, K., 1988. In vitro studies of fretting corrosion of orthopaedic materials. *J. Orthop. Res.* 6 (4), 572–579.
- Brown, S.A., Merritt, K., 1981. In vivo and in vitro considerations of corrosion testing. *Artif. Cells, Blood Substitutes Biotechnol.* 9 (1), 57–63.
- Butt, A., Lucchiari, N.B., Royhman, D., Runa, M.J., Mathew, M.T., Sukotjo, C., et al., 2015. Design, development, and testing of a compact tribocorrosion apparatus for biomedical applications. *J. Bio-Tribo-corros.* [Internet] 1 (1) Available from (<<http://link.springer.com/10.1007/s40735-014-0004-6>>).
- Cao, S., Guadalupe Maldonado, S., Mischler, S., 2015. Tribocorrosion of passive metals in the mixed lubrication regime: theoretical model and application to metal-on-metal artificial hip joints. *Wear* 324–325, 55–63.
- Celis, J.-P., Ponthiaux, P., Wenger, F., 2006. Tribo-corrosion of materials: interplay between chemical, electrochemical, and mechanical reactivity of surfaces. *Wear* 261 (9), 939–946.
- Chandrasekaran, V., Sauer, W.L., Taylor, A.M., Hoepfner, D.W., 1999. Evaluation of the fretting corrosion behavior of the proximal pad taper of a modular hip design. *Wear* 231 (1), 54–64.
- Cook, S.D., Barrack, R.L., Baffes, G.C., Clemow, A.J., Serekian, P., Dong, N., et al., 1994. Wear and corrosion of modular interfaces in total hip replacements. *Clin. Orthop. Relat. Res.* 298, 80–88.
- Cook, R.B., Bolland, B.J.R.F., Wharton, J.A., Tilley, S., Latham, J.M., Wood, R.J.K., 2013. Pseudotumour formation due to tribocorrosion at the taper interface of large diameter metal on polymer modular total hip replacements. *J. Arthroplast.* 28 (8), 1430–1436.
- Cooper, H.J., Urban, R.M., Wixson, R.L., Meneghini, R.M., Jacobs, J. J., 2013. Adverse local tissue reaction arising from corrosion at the femoral neck-body junction in a dual-taper stem with a cobalt-chromium modular neck. *J. Bone Jt. Surg. Am.* 95 (10), 865–872.
- Dufils, J., Laurent, M., Kunze, J., Royhman, D., Mathew, M., Fridrici, V., et al., 2015. A Servo-electric Apparatus with Potentiostat to Study the Fretting Corrosion of Cobalt-Chromium – Titanium Alloy Couples. In: Greenwald, A.S., Kurtz, S.M., Lemons, J.E., Mihalko, W.H. (eds.), *Modularity and Tapers in Total Joint Replacement Devices*. West Conshohocken, PA: ASTM International, pp. 303–320. (ATSM STP1591).
- Fouvry, S., Kapsa, P., Vincent, L., 1995. Analysis of sliding behaviour for fretting loadings: determination of transition criteria. *Wear* 185 (1–2), 35–46.
- Fouvry, S., Paulin, C., Liskiewicz, T., 2007. Application of an energy wear approach to quantify fretting contact durability: Introduction of a wear energy capacity concept. *Tribol. Int.* 40 (10–12), 1428–1440.
- Geringer, J., Atmani, F., Forest, B., 2009. Friction–corrosion of AISI 316L/bone cement and AISI 316L/PMMA contacts: Ionic strength effect on tribological behaviour. *Wear* 267 (5), 763–769.
- Geringer, J., Forest, B., Combrade, P., 2005. Fretting-corrosion of materials used as orthopaedic implants. *Wear* 259 (7–12), 943–951.
- Gilbert, J.L., Buckley, C.A., Jacobs, J.J., 1993. In vivo corrosion of modular hip prosthesis components in mixed and similar metal combinations. The effect of crevice, stress, motion, and alloy coupling. *J. Biomed. Mater. Res.* 27 (12), 1533–1544.
- Gilbert, J.L., Mehta, M., Pinder, B., 2009. Fretting crevice corrosion of stainless steel stem–CoCr femoral head connections: comparisons of materials, initial moisture, and offset length. *J. Biomed. Mater. Res. Part B: Appl. Biomater.* 88 (1), 162–173.
- Goldberg, J.R., Gilbert, J.L., 2004. The electrochemical and mechanical behavior of passivated and TiN/AlN-coated CoCrMo and Ti6Al4V alloys. *Biomaterials* 25 (5), 851–864.
- Griess Jr, J.C., 1968. Crevice corrosion of titanium in aqueous salt solutions. *Corrosion* 24 (4), 96–109.
- Hallab, N.J., Caicedo, M., Epstein, R., McAllister, K., Jacobs, J.J., 2009. In vitro reactivity to implant metals demonstrates a person-dependent association with both T-cell and B-cell activation. *J. Biomed. Mater. Res. Part A* 9999A:NA – NA.
- Hallab, N.J., Merritt, K., Jacobs, J.J., 2001. Metal sensitivity in patients with orthopaedic implants. *J. Bone Jt. Surg.* 83 (3) 428–428.
- Hodgson, A.W.E., Kurz, S., Virtanen, S., Fervel, V., Olsson, C.-O., Mischler, S., 2004. Passive and transpassive behaviour of CoCrMo in simulated biological solutions. *Electrochim. Acta* 49 (13), 2167–2178.
- Huber, M., Reinisch, G., Trettenhahn, G., Zweymüller, K., Lintner, F., 2009. Presence of corrosion products and hypersensitivity-associated reactions in periprosthetic tissue after aseptic loosening of total hip replacements with metal bearing surfaces. *Acta Biomater.* 5 (1), 172–180.
- Hu, P.S., Liu, R., Liu, J., McRae, G., 2014. Investigation of wear and corrosion of a high-carbon stellite alloy for hip implants. *J. Mater. Eng. Perform.* [Internet] Feb 4 [cited 14.02.14]; Available from (<http://link.springer.com/10.1007/s11665-014-0887-x>).
- John Cooper, H., Valle, C.J., Della, Berger, R.A., Tetreault, M., Paprosky, W.G., Sporer, S.M., et al., 2012. Corrosion at the head-neck taper as a cause for adverse local tissue reactions after total hip arthroplasty. *J. Bone Jt. Surg. Am.* 94 (18), 1655–1661.
- Kop, A.M., Swarts, E., 2009. Corrosion of a hip stem with a modular neck taper junction: a retrieval study of 16 cases. *J. Arthroplast.* 24 (7), 1019–1023.
- Kurtz, S.M., Ong, K.L., Lau, E., Bozic, K.J., 2014. Impact of the economic downturn on total joint replacement demand in the United States. *J. Bone Jt. Surg. Am.* 96 (8), 624–630.
- Landolt, D., Mischler, S., Stemp, M., 2001. Electrochemical methods in tribocorrosion: a critical appraisal. *Electrochim. Acta* 46 (24), 3913–3929.
- Lavos-Valereto, I.C., Wolyneec, S., Ramires, I., Guastaldi, A.C., Costa, I., 2004. Electrochemical impedance spectroscopy characterization of passive film formed on implant Ti–6Al–7Nb alloy in Hank’s solution. *J. Mater. Science: Mater. Med.* 15 (1), 55–59.
- Levine, D.L., Staehle, R.W., 1977. Crevice corrosion in orthopedic implant metals. *J. Biomed. Mater. Res.* 11 (4), 553–561.
- Lim, S.C., Ashby, M.F., Brunton, J.H., 1987. Wear-rate transitions and their relationship to wear mechanisms. *Acta Metall.* 35 (6), 1343–1348.

- Mathew, M.T., Jacobs, J.J., Wimmer, M.A., 2012. Wear-corrosion synergism in a CoCrMo hip bearing alloy is influenced by proteins. *Clin. Orthop. Relat. Res.* 470 (11), 3109–3117.
- Mathew, M.T., Patel, M., Royhman, D., Runa, M.J., Jacobs, J.J., Wimmer, M., et al., 2015. Tribocorrosion in Hip Modular Taper Junctions: Load-Triggered Transitions in Electrochemical and Mechanical Behavior. In: Greenwald, A.S., Kurtz, S.M., Lemons, J.E., Mihalko, W.H. (eds.), *Modularity and Tapers in Total Joint Replacement Devices*. West Conshohocken, PA: ASTM International, pp. 283–302. (ATSM STP1591).
- Mischler, S., 2008. Triboelectrochemical techniques and interpretation methods in tribocorrosion: a comparative evaluation. *Tribol. Int.* 41 (7), 573–583.
- Mohrbacher, H., Blanpain, B., Celis, J.-P., Roos, J.R., 1993. Low amplitude oscillating sliding wear on chemically vapour deposited diamond coatings. *Diam. Relat. Mater.* 2 (5), 879–884.
- Oladokun, A., Pettersson, M., Bryant, M., Engqvist, H., Persson, C., Hall, R., et al., 2015. Fretting of CoCrMo and Ti6Al4V alloys in modular prostheses. *Tribol. – Materials, Surf. Interfaces Jun 20;1751584X15Y.000*.
- Pourbaix, M., 1974. Atlas of electrochemical equilibria in aqueous solutions. *NACE*, 644 [Internet] [cited 12.03.13]; Available from: <http://www.csa.com/partners/viewrecord.php?requester=gs&collection=TRD&recid=943388CO>.
- Rodrigues, D.C., Urban, R.M., Jacobs, J.J., Gilbert, J.L., 2009. In vivo severe corrosion and hydrogen embrittlement of retrieved modular body titanium alloy hip-implants. *J. Biomed. Mater. Res. Part B: Appl. Biomater.* 88 (1), 206–219.
- Royhman, D., Patel, Megha, Runa, M.J., Jacobs, J.J., Hallab, N.J., Wimmer, M.A., et al., 2015. Fretting-corrosion in hip implant modular junctions: new experimental set-up and initial outcome. *Tribol. Int.* 91, 235–245.
- Royhman, D., Radhakrishnan, R., Yuan, J.C.-C., Mathew, M.T., Mercuri, L.G., Sukotjo, C., 2014. An electrochemical investigation of TMJ implant metal alloys in an artificial joint fluid environment: the influence of pH variation. *J. Cranio-Maxillofacial Surg.* 42 (7), 105–261.
- Royhman, D., Yuan, J.C., Shokuhfar, T., Takoudis, C., Sukotjo, C., Mathew, M.T., 2013. Tribocorrosive behaviour of commonly used temporomandibular implants in a synovial fluid-like environment: Ti-6Al-4V and CoCrMo. *J. Phys. D: Appl. Phys.* 46 (40), 404002.
- Stack, M.M., Abdulrahman, G.H., 2010. Mapping erosion-corrosion of carbon steel in oil exploration conditions: Some new approaches to characterizing mechanisms and synergies. *Tribol. Int.* 43 (7), 1268–1277.
- Swaminathan, V., Gilbert, J.L., 2012. Fretting corrosion of CoCrMo and Ti6Al4V interfaces. *Biomaterials* 33 (22), 5487–5503.
- Whitehouse, M.R., Endo, M., Zachara, S., Nielsen, T.O., Greidanus, N.V., Masri, B.A., et al., 2015. Adverse local tissue reactions in metal-on-polyethylene total hip arthroplasty due to trunnion corrosion the risk of misdiagnosis. *Bone Jt. J.* 97-B (8), 1024–1030.
- Wimmer, M.A., Laurent, M.P., Mathew, M.T., Nagelli, C., Liao, Y., Marks, L.D., et al., 2015. The effect of contact load on CoCrMo wear and the formation and retention of tribofilms. *Wear* 332–333, 643–649.